On geometry and kinematics of abrasive processes: The theory of aggressiveness

International Journal of Machine Tools & Manufacture 154 (2020) 103567

Contents lists available at ScienceDirect

International Journal of Machine Tools and Manufacture

journal homepage: http://www.elsevier.com/locate/ijmactool

On geometry and kinematics of abrasive processes: The theory of aggressiveness

Radovan Dražumerič [a,b,c], Jeffrey Badger [a,d], Roope Roininen [e], Peter Krajnik [c,*]

[a] The International Grinding Institute, San Antonio, TX, USA
[b] University of Ljubljana, Faculty of Mechanical Engineering, Ljubljana, Slovenia
[c] Chalmers University of Technology, Department of Industrial and Materials Science, Gothenburg, Sweden
[d] The Grinding Doc, San Antonio, TX, USA
[e] Scania CV AB, Södertälje, Sweden

ARTICLE INFO

Keywords:
Abrasive
Geometry
Kinematics
Grinding
Truing
Dressing

ABSTRACT

Due to the stochastic nature of the abrasive-tool topography, abrasive processes are difficult to model and quantify. In contrast, their macro geometry and kinematics are usually well defined and straightforwardly controlled on machine tools. To reconcile this seeming contradiction, a novel unifying modelling framework is defined through the theory of aggressiveness. It encompasses the arbitrary geometry and kinematics of a workpiece moving relative to an abrasive surface. The key parameter is the point-aggressiveness, which is a dimensionless scalar quantity based on the vector field of relative velocity and the vector field of abrasive-surface normals. This fundamental process parameter relates directly to typical process outputs such as specific energy, abrasive-tool wear and surface roughness. The theory of aggressiveness is experimentally validated by its application to a diverse array of abrasive processes, including grinding, diamond truing and dressing, where the aggressiveness number is correlated with the aforementioned measured process outputs.

1. Introduction

The fundamental models used to quantify abrasive processes evolved from metal-cutting theories of chip-formation developed in the 1940s, where the geometry of the cutting edge is well defined and the spacing between edges is easily determined [1–3]. Since these early days, it is often (mis)understood that abrasive processing is simply cutting with a large number of cutting edges, producing small chips. Indeed, while the fundamental concept of specific energy (i.e. energy per unit volume of material removed) is the same for cutting and abrasive processes, there are significant differences in comparison to conventional metal cutting. Abrasive processes use geometrically-undefined cutting edges [4,5] with random geometry and distribution [6] that change during the process due to wear [7,8]. Nevertheless, whichever operation is concerned, advancing the understanding of essential process mechanics typically requires analytical modelling to mathematically describe and correlate process outputs with process geometry and kinematics. For example, a fundamental derivation of chip formation in metal cutting accounting for the operating variables (e.g. feed and speed) would enable the prediction of cutting force, temperature and other process outputs [9].

In grinding, chip formation plays an equally important role, albeit on a smaller scale, as observed as early as 1914 by Alden [10] and 1915 by Guest [11]. The fundamental mechanics of chip formation in abrasive processes, however, is vastly different than in metal cutting. Chip formation occurs through a three-dimensional, large-strain extrusion process to the side of the grit, leaving a long scratch in the workpiece where subsequent abrasives encounter the peak or valley left by some previous grit [12], which in fact facilities chip formation. In addition, many grits do not form a chip, but merely plow or rub. These three interactions produce forces and heat generation that are an order of magnitude greater than those of the chip formation [13]. Whether the grit cuts, rubs or plows depends on the depth that the grit penetrates into the workpiece, typically referred to as the chip thickness. It depends on a multitude of variables, including the grinding-wheel topography and the geometrical parameters and kinematical quantities. Various methods have been used to quantify the chip thickness [14], the most common being the equivalent chip-thickness [15]. This basic model takes into account the kinematic parameters and, to a limited extent, the geometrical parameters. Later, numerous attempts were made to incorporate the stochastic aspects and empirical terms, for example to account for the influence of the grinding-wheel topography. This led to

* Corresponding author.
E-mail address: peter.krajnik@chalmers.se (P. Krajnik).

https://doi.org/10.1016/j.ijmachtools.2020.103567
Received 16 February 2020; Received in revised form 20 April 2020; Accepted 24 April 2020
Available online 25 April 2020

Nomenclature

$Aggr^{*}$	point-aggressiveness
$Aggr^{'}$	line-aggressiveness
$Aggr^{'}_{s}$	line-aggressiveness from abrasive-tool perspective
$Aggr^{'}_{w}$	line-aggressiveness from workpiece perspective
$Aggr$	aggressiveness number
$Aggr_D$	dressing aggressiveness-number
$Aggr_G$	grinding aggressiveness-number
$Aggr_T$	truing aggressiveness-number
a_D	dressing depth
a_T	truing depth
a_n	normal infeed
a_s	depth of cut from abrasive-tool perspective
$a_{s,n}$	normal infeed from abrasive-tool perspective
$a_{s,t}$	tangential infeed from abrasive-tool perspective
a_t	tangential infeed
a_w	depth of cut from workpiece perspective
$a_{w,n}$	normal infeed from workpiece perspective
$a_{w,t}$	tangential infeed from workpiece perspective
a_x	radial infeed
a_z	axial infeed
C	cutting-point density
C_0	coefficient independent of profile position
$C_{\cos}$	coefficient related to cosine
$C_{\sin}$	coefficient related to sine
e	specific energy
e_D	dressing specific-energy
e_G	grinding specific-energy
$e_{eq,G}$	equivalent grinding specific-energy
$\vec{F}_t$	tangential-force vector
$\vec{F}^{'}_t$	specific tangential-force vector
G_T	truing ratio
h	undeformed chip-thickness
h_{eq}	equivalent chip-thickness
$h_{eq,D}$	dressing equivalent chip-thickness
$h_{eq,G}$	grinding equivalent chip-thickness
l_c	contact length
$l_{c,s}$	contact length from abrasive-tool perspective
$l_{c,w}$	contact length from workpiece perspective
$\vec{n}$	abrasive-tool surface normal
P	power
P_D	dressing power
P_G	grinding power
$Q^{'}$	specific material-removal rate
$Q^{'}_D$	dressing specific material-removal rate
$Q^{'}_s$	specific material-removal rate from abrasive-tool perspective
$Q^{'}_w$	specific material-removal rate from workpiece perspective
Q	material-removal rate
Q_D	dressing material-removal rate
Q_G	grinding material-removal rate
q	speed ratio
q_D	dressing speed-ratio
q_T	truing speed-ratio
Ra_G	grinding roughness
$\mathrm{Ra}_{eq,G}$	equivalent grinding roughness
r	chip-shape factor
r_{eq}	equivalent radius
r_s	abrasive-tool radius
r_w	workpiece radius
S_c	contact surface
s	abrasive-tool profile position
$s_{\max}$	maximum value of wheel-profile position
$s_{s,0}$	lower bound of singular region from abrasive-tool perspective
$s_{s,1}$	upper bound of singular region from abrasive-tool perspective
$s_{w,0}$	lower bound of singular region from workpiece perspective
$s_{w,1}$	upper bound of singular region from workpiece perspective
$\vec{v}$	relative-velocity vector
$\vec{v}_n$	normal relative-velocity vector
$\vec{v}_s$	abrasive-tool relative-velocity vector
$\vec{v}_t$	tangential relative-velocity vector
$\vec{v}_w$	workpiece relative-velocity vector
v_f	traverse velocity
v_n	normal relative-velocity
v_s	abrasive-tool relative velocity
v_t	tangential relative-velocity
v_w	workpiece relative velocity
w_D	dressing width
w_T	truing width
x, y, z	global coordinate system
x_s, y_s, z_s	abrasive-tool local coordinate system
x_w, y_w, z_w	workpiece local coordinate system
α	swivel angle of rotational axes
Δs_s	profile-position difference in abrasive-tool coordinate system
Δs_w	profile-position difference in workpiece coordinate system
η_T	truing efficiency
ϑ	tangent angle of abrasive-tool profile
ρ	curvature radius of abrasive-tool profile
ρ_0	fillet radius
$\vec{\tau}$	shear vector
τ	shear of abrasive interaction
ω_s	abrasive-tool rotational speed
ω_w	workpiece rotational speed

ongoing confusion, including: i) the level of detail to be included in a model; ii) a multitude of equations for different processes and geometries [14]; iii) the use of average values or maximum values for different positions in the grit path; and, perhaps most confusingly, iv) complications arising from the need to quantify the seemingly random spacing and micro-geometry of abrasive-surface topography [15–17].

In contrast, quantifying only the deterministic aspects of abrasive processes such as geometry and kinematics – and not considering, for example, the stochastic topography of the abrasive surface – leads to less ambiguity and eliminates the estimation/measures required for quantifying the topography of the abrasive surface. The first known attempt to quantify the dimensionless portion of chip thickness, which considers only geometry and kinematics of plunge grinding, was by Brecker and Shaw [18], who used the term $(v/V)\cdot(d/D)^{0.5}\cdot 10^6$, where v is the workpiece speed, V is the wheel speed, d is the depth of cut, and D is the wheel diameter, with the 10^6 constant chosen to give more graspable values. Later, for cylindrical grinding process, Malkin and Guo [13] defined the degree of interference at any location along the cutting path by tangent of the infeed angle ε between the peripheral velocity vector and the workpiece velocity vector. In rotary diamond dressing, Malkin and Murray [19] considered the tangent of the interference angle δ which the trochoidal path of the diamond grit makes relative to the

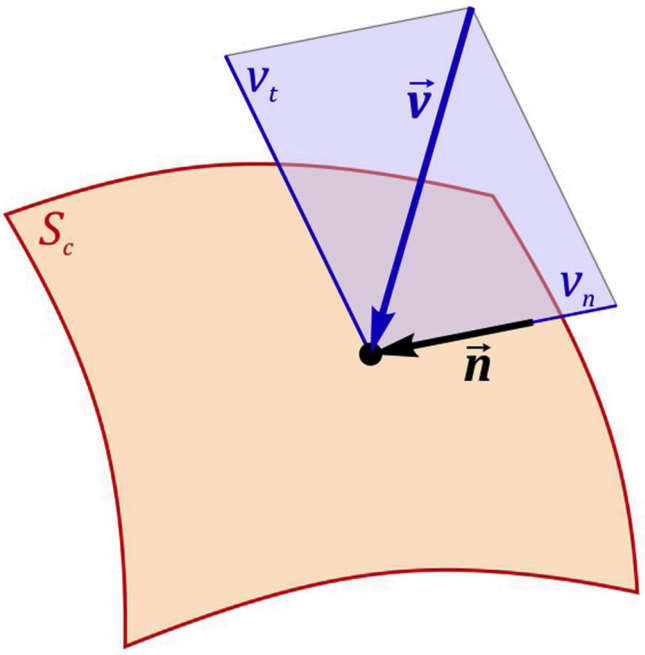

Fig. 1. Relative-velocity vector and its components at point of contact surface.

grinding wheel periphery as the diamond passes through the contact length between the rotary dresser and the grinding wheel. Note again that such dimensionless approaches are concerned strictly with the geometry and kinematics of the process and do not necessitate the consideration of the stochastic nature of the abrasive interaction [20], nor do they require numerical methods for quantifying the (micro) topography of the interacting abrasive surface(s). This stands in stark contrast to the "overdetermined" modelling approach dominating much of the grinding research [21], which results in the introduction of an overwhelmingly large number of empirical parameters and constants, almost all of which are unknown. This adds incredible complexity to process modelling. To further complicate matters, additional parameters may be added *ad nauseum* in an attempt to further quantify the abrasive-surface topography. In contrast, it is possible to explain the basic features of, for example, double-disc grinding kinematics and resulting workpiece geometry by using a model without any tool-specific assumptions and without any model-fitting parameters [22].

One might argue that such an approach is limited, but recent applications of aggressiveness number in modelling the geometry and kinematics of camshaft [23] and crankshaft grinding [24] proved effective in advancing both understanding and optimizing these processes – for example, to achieve reductions in thermal damage and cycle time – without requiring any attempt to quantify the abrasive-surface topography, however inaccurately. In addition, the use of dimensionless aggressiveness in modelling a truing process [25] led to a better understanding of the fundamental truing mechanism and parameters. Most strikingly, this approach is universal and is not limited to the cases above. It can be applied to any two contacting abrasive surfaces. Further applications may include but are not limited to optimization of cylindrical and centerless grinding based on variable speeds [26], thermal modelling and optimization of interrupted grinding [27], and modelling of gear grinding [28].

The overall objective of this paper is to unify the multitude of modelling approaches and specifically to provide new fundamental dimensionless parameters for modelling of abrasive processes through the theory of aggressiveness. The theory encompasses all possible geometries and kinematics of any abrasive process via a dimensionless parameter, enabling the study of fundamental process mechanics. This will be useful to other researchers and practitioners analyzing and optimizing future abrasive processes.

2. Theory of aggressiveness

In this section, the dimensionless parameters which comprise the theory of aggressiveness are established. The general definition associates an abrasive interaction at a given contact point with the kinematical process parameters and the abrasive-contact geometry.

First, the surface of an abrasive tool is represented by the vector field of surface normals, $\vec{n}$ (Fig. 1). Next, the vector field of relative velocity, $\vec{v}$, incorporates the kinematics of both the abrasive tool and the workpiece. The fundamental parameter of the abrasive interaction, termed the point-aggressiveness, $Aggr^*$, is defined as the ratio of the normal component, v_n, and the tangential component, v_t, of the relative-velocity vector:

$$Aggr^* = \frac{v_n}{v_t} = \frac{\vec{v}\cdot\vec{n}}{\sqrt{\vec{v}\cdot\vec{v} - (\vec{v}\cdot\vec{n})^2}}. \tag{1}$$

The point-aggressiveness represents a scalar field on the abrasive-tool surface. Geometrically, the point-aggressiveness can be interpreted as the tangent of an angle at which a given point of the workpiece penetrates into the abrasive tool.

While the point-aggressiveness quantifies an abrasive interaction in terms of geometry and kinematics at a given point on the abrasive-tool surface, the concept can be broadened out to a contact line in the abrasive contact. The line-aggressiveness, $Aggr'$, is defined as the average point-aggressiveness along a pre-defined contact curve:

$$Aggr' = \frac{1}{l_c}\int_{l_c} Aggr^* \mathrm{d}l_c, \tag{2}$$

where l_c is the contact length.

The concept can finally be broadened out to the entire abrasive contact. The aggressiveness number, $Aggr$, is defined as the average point-aggressiveness over the contact area, S_c:

$$Aggr = \frac{1}{S_c}\iint_{S_c} Aggr^* \mathrm{d}S_c. \tag{3}$$

Although the defined parameter in the above equation geometrically represents surface aggressiveness, the term *aggressiveness number* is used to emphasize the overall characteristic of the abrasive contact, where one characteristic number corresponds to a given contact.

A unique characteristic of the point-aggressiveness as the fundamental process parameter is that it relates directly to the shear of the abrasive interaction, τ. The shear vector, $\vec{\tau}$, written by its magnitude, τ, in the direction of the tangential velocity, is defined as:

$$\vec{\tau} = \frac{\vec{v}_t}{v_t}\tau = \frac{d\vec{F}_t}{dS_c}, \tag{4}$$

where $\vec{F}_t$ is the tangential-force vector and $\vec{v}_t$ is the tangential-velocity vector, expressed with the normal-velocity vector, $\vec{v}_n$, as:

$$\vec{v}_n = (\vec{v}\cdot\vec{n})\cdot\vec{n}, \quad \vec{v}_t = \vec{v} - \vec{v}_n. \tag{5}$$

Using Eq. (4) with the differential form of the specific energy, e, in an abrasive process, the following relation to the shear is obtained:

$$e = \frac{dP}{dQ} = \tau\frac{v_t}{v_n}, \tag{6}$$

where $dP = \vec{v}_t\cdot d\vec{F}_t$ is the power differential and $dQ = v_n dS_c$ is the material-removal rate differential. Therefore, according to the definition of the point-aggressiveness in Eq. (1), the shear at any point of the

Table 1
Relation of the theory of aggressiveness to established abrasive-process parameters.

Established abrasive-process parameters	Relation to the theory of aggressiveness
Specific material-removal rate	$Q^{'} = \int_{l_c} v_n \mathrm{d}l_c$
Material-removal rate	$Q = \iint_{S_c} v_n \mathrm{d}S_c$
Equivalent chip-thickness	$h_{eq} = \int_{l_c} Aggr^* \mathrm{d}l_c = l_c\, Aggr^{'}$
Undeformed chip-thickness	$h = \sqrt{\frac{4}{Cr} Aggr^*}$
Specific tangential force	$\vec{F}_t^{'} = \int_{l_c} \frac{\vec{v}_t}{v_t} e\, Aggr^* \mathrm{d}l_c$
Tangential force	$\vec{F}_t = \iint_{S_c} \frac{\vec{v}_t}{v_t} e\, Aggr^* \mathrm{d}S_c$

abrasive contact is simply calculated as:

$$\tau = e\, Aggr^*. \tag{7}$$

Over time, several parameters have been proposed to advance a fundamental understanding of an abrasive interaction. The theory of aggressiveness unifies the geometric and kinematical aspects of any abrasive process. A summary of the relationships between well-established parameters [13] (concerned with e.g. material-removal rate, chip thickness and grinding force) and the theory of aggressiveness is given in Table 1, where C is the cutting-point density of an abrasive tool and r is the chip-shape factor. In the experimental section, the results for various abrasive processes show that the main characteristics of an abrasive process, such as specific energy, abrasive-tool wear and surface roughness, depend exclusively on the aggressiveness of the process.

2.1. Fundamental derivation

In this section, the derivation of the fundamental relations within the theory of aggressiveness is conducted. The relations apply to an abrasive contact according to the following features:

- The abrasive tool is rotating with a rotational speed ω_s and the workpiece is rotating with a rotational speed ω_w (Fig. 2).
- The abrasive tool is rotationally symmetric and its intersection with the plane $x-z$ of the global coordinate system (x, y, z) represents the abrasive-tool profile (Figs. 2a and 3a). Therefore, the abrasive-tool profile position, s, is used as the main independent variable.
- The rotational axes of an abrasive tool and a workpiece lie in the same plane and are swiveled at an angle α (Fig. 3a), where $0 \leq \alpha \leq \pi/2$.
- An abrasive interaction is achieved by the radial infeed, a_x, and the axial infeed, a_z (Fig. 3b), which are given per rotation of the workpiece (i.e. feed increment). The values of the infeeds are on a much smaller scale compared to the radius of the abrasive tool, r_s, and the radius of the workpiece, r_w. Therefore, all terms of higher order with respect to the infeeds and the dimensions of an abrasive contact are neglected in the subsequent relations. The abrasive-tool profile is given by the simplified relations using the tangent angle, ϑ, and the radius of profile curvature, ρ, in the point s (Fig. 3a). The tangent angle lies in the interval $0 \leq \vartheta \leq \pi/2$, and the radius ρ can have positive or negative values. A positive value of the curvature radius means a convex shape of the profile and a negative value of the curvature radius means a concave shape.
- The path through the abrasive contact that corresponds to the point s can be observed from the two perspectives (Fig. 2b). The first is the abrasive-tool perspective, where $l_{c,s}$ is the contact length from the abrasive-tool perspective. The second is the workpiece perspective, where $l_{c,w}$ is the contact length from the workpiece perspective. Note that in the case where a total infeed has a tangential component, the contact exit-point from the workpiece perspective is shifted from the corresponding point s for the magnitude of this component (Fig. 2b).

From the abrasive-tool perspective, a point on the abrasive-tool surface is followed through the abrasive contact, whereas from the workpiece perspective a point on the workpiece surface is followed through the abrasive contact. In both cases, following a point through the contact forms a corresponding curve on the contact surface depending on a chosen point of the abrasive-tool profile position. The abrasive-tool perspective is relevant for analyzing phenomena such as the abrasive-tool wear; whereas the workpiece perspective is relevant for other phenomena – such as thermal damage or surface roughness. Therefore, this unique two-perspective approach – in conjunction with the theory of aggressiveness, which is applicable to any geometry and kinematics of any abrasive process – is the main contribution of this paper.

Considering the defined features of an abrasive contact, the point-aggressiveness, given in Eq. (1), can now be calculated in the abrasive-tool local coordinate system (x_s, y_s, z_s), which originates in the point s of the abrasive-tool profile (Fig. 3b). The essential kinematics here is fully captured by the relative-velocity vector:

$$\vec{v} = \vec{v}_s + \vec{v}_w. \tag{8}$$

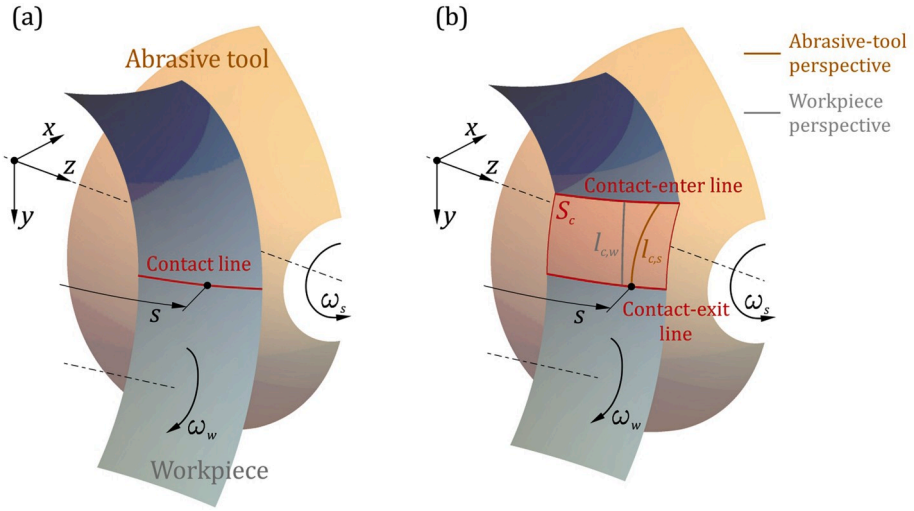

Fig. 2. 3D geometry and kinematics of abrasive interaction (a) before and (b) after abrasive-tool infeed.

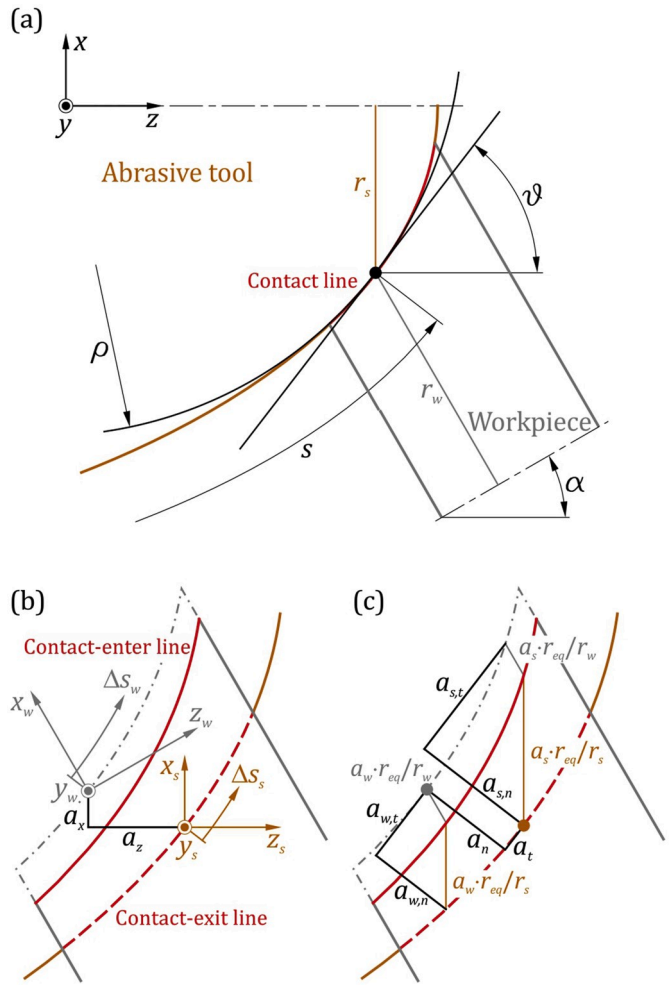

Fig. 3. 2D geometry of abrasive interaction at abrasive-tool profile (a) before and after abrasive-tool infeed with (b) local coordinate systems and (c) characteristic infeeds.

The abrasive-tool relative-velocity vector, $\vec{v}_s$, is calculated by:

$$\vec{v}_s = v_s\left(\frac{y_s}{r_s}, 1, 0\right);\ v_s = r_s\omega_s, \tag{9}$$

where v_s is the abrasive-tool velocity at point s. The workpiece relative-velocity vector, $\vec{v}_w$, is calculated by:

$$\vec{v}_w = v_w\left(\frac{y_s}{r_w}\cos\alpha, -1, -\frac{y_s}{r_w}\sin\alpha\right);\ v_w = r_w\omega_w, \tag{10}$$

where v_w is the workpiece velocity at point s.

The abrasive-tool geometry at point s is given in a simplified form as:

$$\begin{aligned} x_s &= \Delta s_s \sin\vartheta + \frac{\Delta s_s^2}{2\rho}\cos\vartheta + \frac{y_s^2}{2r_s}, \\ z_s &= \Delta s_s \cos\vartheta - \frac{\Delta s_s^2}{2\rho}\sin\vartheta, \end{aligned} \tag{11}$$

where Δs_s is the profile-position difference in the abrasive-tool coordinate system (Fig. 3b). The corresponding normal vector is:

$$\vec{n} = \left(\cos\vartheta, -\frac{y_s}{r_s}\cos\vartheta, -\sin\vartheta\right) - \frac{\Delta s_s}{\rho}\left(\sin\vartheta, -\frac{y_s}{r_s}\sin\vartheta, \cos\vartheta\right). \tag{12}$$

Now, the components of the relative-velocity vector can be determined as:

$$v_n = \vec{v}_w \cdot \vec{n} = v_w\frac{y_s}{r_{eq}}\left(C_{\cos} - \frac{\Delta s_s}{\rho}C_{\sin}\right),\ v_t = |v_w - v_s|, \tag{13}$$

where the coefficients in the given equation are:

$$C_{\cos} = \frac{r_w\cos\vartheta + r_s\cos(\vartheta-\alpha)}{r_w + r_s}, C_{\sin} = \frac{r_w\sin\vartheta + r_s\sin(\vartheta-\alpha)}{r_w + r_s}, \tag{14}$$

and $r_{eq} = r_w r_s/(r_w + r_s)$ is the equivalent radius. Furthermore, the coefficient C_0, which implies the relationship between the coefficients in Eq. (14) that does not depend on the abrasive-tool profile position s, can be defined as:

$$C_0^2 = C_{\cos}^2 + C_{\sin}^2 = 1 - \frac{2r_{eq}}{r_w + r_s}(1 - \cos\alpha) \tag{15}$$

Finally, the point-aggressiveness of the abrasive tool around the profile position s is calculated by:

$$Aggr^* = \frac{1}{|1-q|}\frac{y_s}{r_{eq}}\left(C_{\cos} - \frac{\Delta s_s}{\rho}C_{\sin}\right), \tag{16}$$

where $q = v_s/v_w$ is the speed ratio.

In order to bring the theory of aggressiveness to an abrasive contact, the contact boundaries must be determined. Before the abrasive-tool infeed, the interaction between the abrasive tool and the workpiece is represented by the contact line at $y_s = 0$ (Figs. 2a and 3a). After the infeed, the abrasive contact is determined by the contact-enter line and the contact-exit line (Figs. 2b and 3b). Since the contact-exit line coincides with the contact line at $y_s = 0$, only the contact-enter line is calculated. Similar to the abrasive-tool geometry in its local coordinate system, defined in Eq. (11), the workpiece geometry around the point that corresponds to the abrasive-tool profile position s is determined in the workpiece local coordinate system (x_w, y_w, z_w) as:

$$\begin{aligned} x_w &= \Delta s_w \sin(\vartheta-\alpha) + \frac{\Delta s_w^2}{2\rho}\cos(\vartheta-\alpha) - \frac{y_w^2}{2r_w}, \\ z_w &= \Delta s_w \cos(\vartheta-\alpha) - \frac{\Delta s_w^2}{2\rho}\sin(\vartheta-\alpha), \end{aligned} \tag{17}$$

where Δs_w is the profile-position difference in the workpiece coordinate system (Fig. 3b). Now, Eqs. (11) and (17) are used in the relation between the abrasive-tool and the workpiece coordinate systems:

$$x_s = x_w\cos\alpha + z_w\sin\alpha + a_x,\ y_s = y_w,\ z_s = -x_w\sin\alpha + z_w\cos\alpha - a_z, \tag{18}$$

and the following conditional equations of the contact-enter line are obtained:

$$\frac{y_s^2}{2r_{eq}}C_{\cos} = \frac{\Delta s_w^2 - \Delta s_s^2}{2\rho} + a_n,\ \frac{y_s^2}{2r_{eq}}C_{\sin} = \Delta s_w - \Delta s_s - a_t, \tag{19}$$

where the normal infeed, a_n, and the tangential infeed, a_t, (Fig. 3c) are calculated as:

$$a_n = a_x\cos\vartheta + a_z\sin\vartheta,\ a_t = -a_x\sin\vartheta + a_z\cos\vartheta. \tag{20}$$

2.2. Line-aggressiveness from abrasive-tool perspective

Observing from the abrasive-tool perspective at a given point s means following a point on the abrasive-tool surface through the abrasive contact. The resulting curve is described in the abrasive-tool local coordinate system by Eq. (11) for $\Delta s_s = 0$. The corresponding coordinate y_s of the contact-enter line represents the contact length from the abrasive-tool perspective ($y_s = l_{c,s}$), which is calculated as:

$$l_{c,s} = \sqrt{2r_{eq}a_s}, \tag{21}$$

Table 2
Depth of cut from abrasive-tool perspective.

General expression	
$a_s = \frac{\rho}{C_{\sin}^2}\left(C_{\cos} - \sqrt{C_{\cos}^2 - 2\frac{a_n}{\rho}C_{\sin}^2}\right)$	
Limit case	
Condition	Expression
$\frac{C_{\sin}^2}{\rho}\to 0 \cap C_{\cos} > 0$	$a_s = \frac{a_n}{C_{\cos}}$
Singular case	
Condition	Expression
$C_{\cos}^2 < 2\frac{a_n}{\rho}C_{\sin}^2 \cup \left(\frac{C_{\sin}^2}{\rho}\to 0 \cap C_{\cos}\to 0\right)$	$a_s = s_{s,1} - s + a_s(s_{s,1});\ s_{s,0} < s < s_{s,1}$

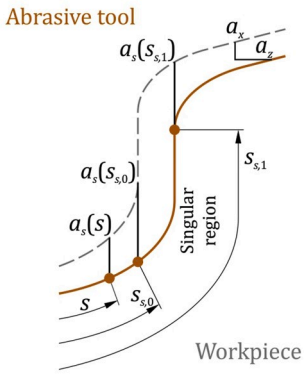

Fig. 4. Illustration of depth of cut from abrasive-tool perspective with related parameters.

Table 3
Depth of cut from workpiece perspective.

General expression	
$a_w = \frac{\rho}{C_{\sin}^2}\left(-C_{\cos} + \sqrt{C_{\cos}^2 + 2\frac{a_n}{\rho}C_{\sin}^2}\right)$	
Limit case	
Condition	Expression
$\frac{C_{\sin}^2}{\rho}\to 0 \cap C_{\cos} > 0$	$a_w = \frac{a_n}{C_{\cos}}$
Singular case	
Condition	Expression
$C_{\cos}^2 < -2\frac{a_n}{\rho}C_{\sin}^2 \cup \left(\frac{C_{\sin}^2}{\rho}\to 0 \cap C_{\cos}\to 0\right)$	$a_w = s - s_{w,0} + a_w(s_{w,0});\ s_{w,0} < s < s_{w,1}$

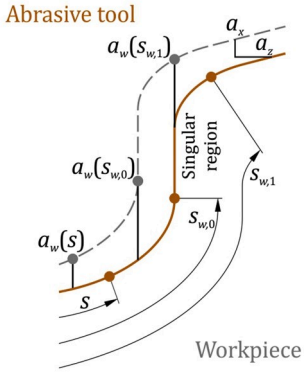

Fig. 5. Illustration of depth of cut from workpiece perspective with related parameters.

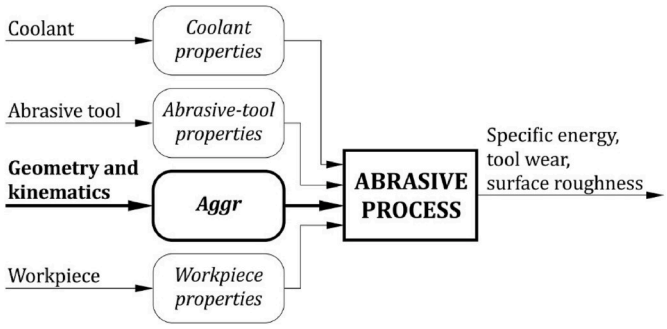

Fig. 6. Role of aggressiveness number in abrasive-process modelling.

Table 4
Case-studies demonstrating applicability of theory of aggressiveness.

Abrasive process	Abrasive tool	Workpiece
Grinding of crankshafts	CBN wheel	Crankpin (steel)
Truing of diamond wheels[a]	Truing wheel (Al_2O_3)	Diamond wheel
Dressing of CBN wheels	Diamond dresser	CBN wheel

[a] In truing of diamond wheels the consumption of abrasive tool is much larger than the workpiece, hence a diamond wheel is considered an abrasive tool from the modelling perspective.

where a_s is the depth of cut from the abrasive-tool perspective. Based on Eq. (19), the general expression for a_s is given in Table 2, along with the possible limit and singular case, where $s_{s,0}$ and $s_{s,1}$ are bounds of a singular region. The depth of cut from the abrasive-tool perspective as a function of s with the example of a singular region is illustrated in Fig. 4.

Using the depth of cut from the abrasive-tool perspective determined by Table 2, the normal and tangential infeeds from the abrasive-tool perspective (Fig. 3c) are calculated as:

$$a_{s,n} = a_s C_{\cos},\ a_{s,t} = a_s C_{\sin}. \tag{22}$$

The profile-position difference of the contact-enter point in the workpiece coordinate system can be determined by combining Eq. (19) and Eq. (22) as:

$$\Delta s_w = a_{s,t} + a_t. \tag{23}$$

Based on the definition in Table 1 and Eq. (13), the specific material-removal rate from the abrasive-tool perspective is:

$$Q_s^{'} = \int_0^{l_{c,s}} v_w \frac{y_s}{r_{eq}} C_{\cos} \mathrm{d}y_s. \tag{24}$$

After the integration, using Eq. (21) and Eq. (22), the following expression is obtained:

$$Q_s^{'} = v_w a_{s,n}. \tag{25}$$

Finally, introducing Eq. (16) into the definition given by Eq. (2), the line-aggressiveness from the abrasive-tool perspective is calculated as:

$$Aggr_s^{'} = \frac{1}{l_{c,s}} \int_0^{l_{c,s}} \frac{1}{|1-q|} \frac{y_s}{r_{eq}} C_{\cos} \mathrm{d}y_s, \tag{26}$$

which together with Eq. (21) and Eq. (22) gives the final expression for the line-aggressiveness from the abrasive-tool perspective:

$$Aggr_s^{'} = \frac{1}{|1-q|} \frac{a_{s,n}}{l_{c,s}}. \tag{27}$$

2.3. Line-aggressiveness from workpiece perspective

The other relevant observation-perspective at a given point s is the workpiece perspective. Here, a point on the workpiece surface is

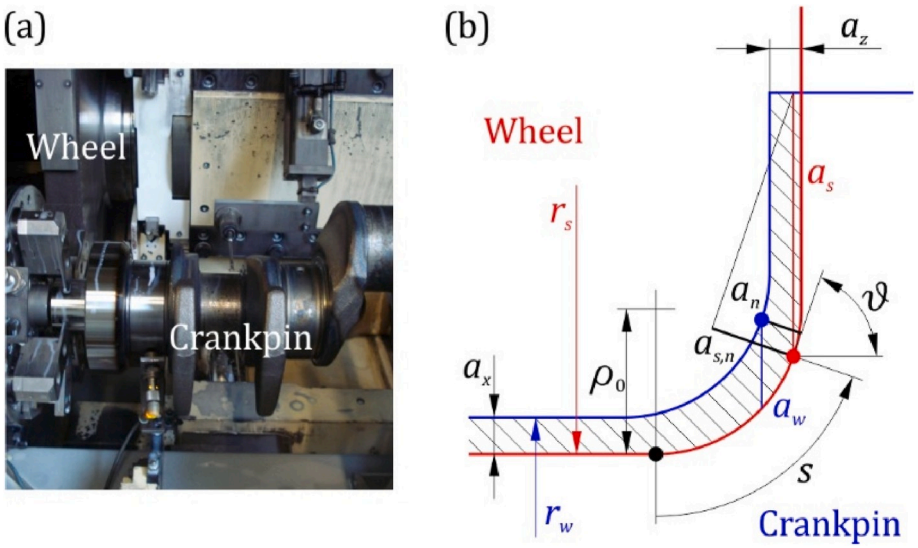

Fig. 7. (a) Crankpin grinding with (b) illustration and parameters.

Table 5
Depth of cut and line-aggressiveness along wheel profile from wheel and workpiece (crankpin) perspective.

Wheel-profile interval	Depth of cut	Line-aggressiveness
Wheel perspective		
$s \le 0$	$a_s = a_x$	$Aggr_s^{'} = \frac{1}{\lvert 1-q\rvert}\sqrt{\frac{a_x}{2r_{eq}}}$
$0 < s \le \frac{\pi}{2}\rho_0 - \sqrt{2\rho_0 a_z}$	$a_s = \frac{\rho_0}{\sin^2\frac{s}{\rho_0}}\left(\cos\frac{s}{\rho_0} - \sqrt{\cos^2\frac{s}{\rho_0} - 2\frac{a_n}{\rho_0}\sin^2\frac{s}{\rho_0}}\right)$	$Aggr_s^{'} = \frac{1}{\lvert 1-q\rvert}\sqrt{\frac{a_s}{2r_{eq}}\cos\frac{s}{\rho_0}}$
$\frac{\pi}{2}\rho_0 - \sqrt{2\rho_0 a_z} < s \le \frac{\pi}{2}\rho_0$	$a_s = s_{\max} - s$	
$\frac{\pi}{2}\rho_0 < s$		$Aggr_s^{'} = 0$
Workpiece perspective		
$s \le 0$	$a_w = a_x$	$Aggr_w^{'} = \frac{1}{\lvert 1-q\rvert}\sqrt{\frac{a_x}{2r_{eq}}}$
$0 < s \le \frac{\pi}{2}\rho_0$	$a_w = \frac{\rho_0}{\sin^2\frac{s}{\rho_0}}\left(-\cos\frac{s}{\rho_0} + \sqrt{\cos^2\frac{s}{\rho_0} + 2\frac{a_n}{\rho_0}\sin^2\frac{s}{\rho_0}}\right)$	$Aggr_w^{'} = \frac{1}{\lvert 1-q\rvert}\frac{a_n}{\sqrt{2r_{eq}a_w}}$
$\frac{\pi}{2}\rho_0 < s$	$a_w = s - \frac{\pi}{2}\rho_0 + \sqrt{2\rho_0 a_z}$	$Aggr_w^{'} = \frac{1}{\lvert 1-q\rvert}\frac{a_z}{\sqrt{2r_{eq}a_w}}$

followed through the abrasive contact. The resulting curve is described in the workpiece local coordinate system by Eq. (17) for $\Delta s_w = 0$. The corresponding coordinate y_w of the contact-enter line represents the contact length from the workpiece perspective ($y_w = y_s = l_{c,w}$), which is calculated as:

$$l_{c,w} = \sqrt{2r_{eq}a_w}, \tag{28}$$

where a_w is the depth of cut from the workpiece perspective. The general expression for a_w is also derived from Eq. (19) and given in Table 3, along with the possible limit and singular case, where $s_{w,0}$ and $s_{w,1}$ are bounds of a singular region. The depth of cut from the workpiece perspective as a function of s with the example of a singular region is illustrated in Fig. 5.

Comparing the depths of cut from the two discussed perspectives, it can be found that significant differences between them are in singular regions: if the depth of cut from one perspective increases with s, the other will decrease, while the relationship between them at the bounds of singular regions are $a_w(s_{w,0}) = a_s(s_{s,0})$ and $a_w(s_{w,1}) = a_s(s_{s,1})$.

Using the depth of cut from the workpiece perspective determined by Table 3, the normal and tangential infeeds from the workpiece perspective (Fig. 3c) are calculated as:

$$a_{w,n} = a_w C_{\cos},\ a_{w,t} = a_w C_{\sin}. \tag{29}$$

Combining Eq. (19) and Eq. (29), the profile-position difference of the contact-enter point in the abrasive-tool coordinate system can be determined as:

$$\Delta s_s = -a_{w,t} - a_t. \tag{30}$$

In consideration of the workpiece perspective, the calculation of $Q_w^{'}$ should also take into account a variation of Δs_s along the integration line, given by Eq. (30). Together with the definition in Table 1 and Eq. (13), the following integral form is obtained:

$$Q_w^{'} = \int_0^{l_{c,w}} v_w \frac{y_s}{r_{eq}}\left[C_{\cos} + \frac{1}{\rho}\left(\frac{y_s^2}{2r_{eq}}C_{\sin} + a_t\right)C_{\sin}\right]\mathrm{d}y_s. \tag{31}$$

Using the relations from Table 3 with Eq. (28), the specific material-removal rate from the workpiece perspective is calculated as:

$$Q_w^{'} = v_w a_n. \tag{32}$$

Note that in this case, the expression contains the normal infeed, which depends only on the abrasive-tool tangent angle in the observed point s and the given infeeds a_x, a_z.

The derivation of the line-aggressiveness again uses Eq. (16) with the

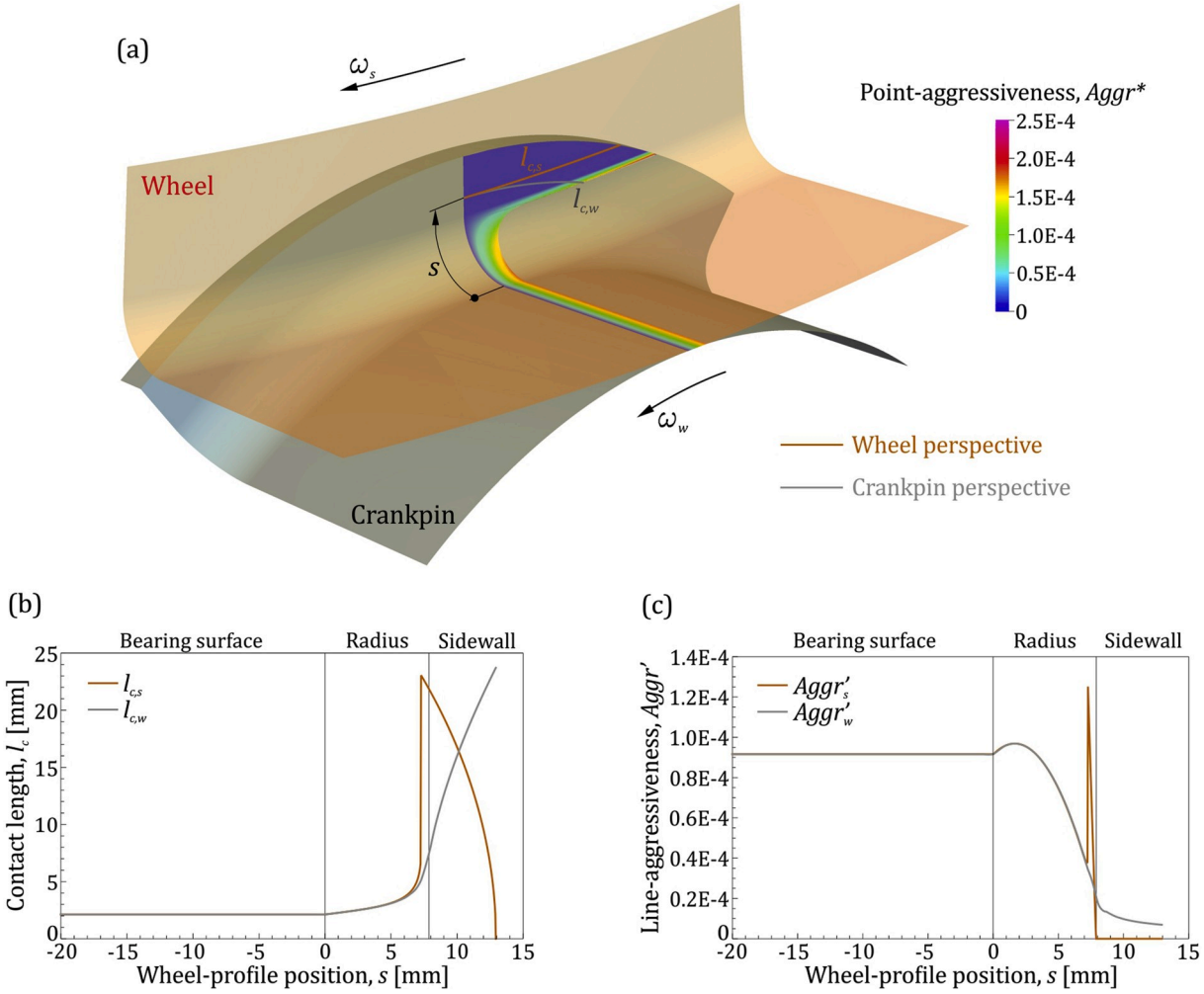

Fig. 8. Crankpin grinding: (a) illustration of point-aggressiveness with charts of (b) contact length and (c) line-aggressiveness depending on wheel-profile position.

definition in Eq. (2). However, in the case of the workpiece perspective, the difference Δs_s (Eq. (30)) should also be included, which gives:

$$Aggr'_w = \frac{1}{l_{c,w}} \int_0^{l_{c,w}} \frac{1}{|1-q|} \frac{y_s}{r_{eq}} \left[C_{\cos} + \frac{1}{\rho} \left(\frac{y_s^2}{2r_{eq}} C_{\sin} + a_t \right) C_{\sin} \right] \mathrm{d}y_s. \tag{33}$$

After the integration, considering Table 3 and Eq. (28), the final form of the line-aggressiveness from the workpiece perspective is obtained as:

$$Aggr'_w = \frac{1}{|1-q|} \frac{a_n}{l_{c,w}}. \tag{34}$$

3. Application of theory of aggressiveness to abrasive processes and experimental validation

Before embarking on validation based on case-studies, the overall objective for the modelling framework needs to be clarified. The level of detail included in the theory of aggressiveness is limited to geometry and kinematics. Specifically, the objective of applying the theory of aggressiveness is to demonstrate clearly that the aggressiveness number is fundamental process parameter in terms of geometry and kinematics for any abrasive operation and is essential for the analysis of key process outputs.

While recognizing that the outputs of an abrasive process always depend on the coolant, abrasive tool (e.g. wheel specification) and workpiece (e.g. hardness, microstructure), the abrasive interaction in a contact is fundamentally determined by the input geometry and kinematics. In this analytical context focusing solely on geometry and kinematics, the (first principle) application of the aggressiveness number captures the correlation of process outputs such as specific energy, tool wear, surface roughness with the process geometry and kinematics (as conceptualized in Fig. 6). Consequently, the analytical models of the theory of aggressiveness account for the fundamental process mechanics. Empirical models, however, do not contribute to the understanding of essential mechanisms. Instead, they only add a certain level of precision to account for changes associated with different properties of coolant, abrasive tool and workpiece.

To illustrate this in detail, three case-studies are presented, each concerned with a distinct abrasive process, i.e. grinding, truing and dressing (Table 4). The results of experimental validation are intended to demonstrate that the key outputs of distinct abrasive processes with different geometry and kinematics depend exclusively on the aggressiveness number as single-valued functions – if and only if geometrical and kinematical process-parameters (operating variables) are varied. A single-valued function means that only one value of a function corresponds to a given value of variable.

3.1. Grinding of crankshafts

The major challenge in grinding of crankshafts (Fig. 7a) is to prevent grinding-induced thermal damage, specifically on the crankpin sidewalls [24]. The high temperatures that cause thermal damage fundamentally depend on the grinding specific-energy, determined as a ratio of grinding power and material removal rate, $e_G = P_G/Q_G$.

The geometry of crankpin grinding along with all the geometrical

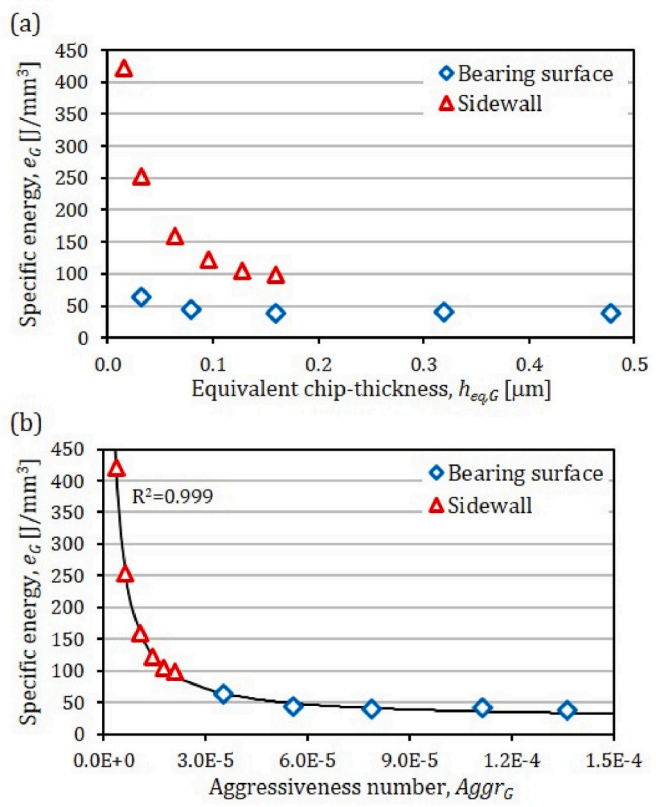

Fig. 9. Grinding specific-energy vs. (a) equivalent chip-thickness and (b) aggressiveness number.

variables required by the theory of aggressiveness is shown in Fig. 7b. Here, the wheel and crankpin axes are parallel, which means $\alpha = 0 \Rightarrow C_{\sin} = \sin\vartheta$, $C_{\cos} = \cos\vartheta$. Note also that the wheel profile is mostly flat, hence the radius of the profile curvature is $\rho \to \infty$, except in the fillet radius, where $\rho = \rho_0$.

The general equations for the depth of cut and the line-aggressiveness from both perspectives, given in the theoretical section, are written for the particular case of crankpin grinding (Table 5), where $s_{\max}$ is the maximum value of the wheel-profile position in a grinding contact.

For the geometry and kinematics that has been used in the grinding experiments ($r_s = 350$ mm, $r_w = 46.5$ mm, $\rho_0 = 5$ mm, $s_{\max} = 12.9$ mm, $v_s = 70$ m/s, $v_w = 223$ mm/s) with the infeeds $a_x = 0.05$ mm and $a_z = 0.03$ mm, the calculations of the point-aggressiveness (Fig. 8a), the contact length (Fig. 8b) and the line-aggressiveness (Fig. 8c) are conducted. Fig. 8a also shows the contact length from both perspectives at the grinding sidewall ($s = 9$ mm). The main result of these calculations is the line-aggressiveness along the wheel profile from both perspectives, which could be used as the basis for the process optimization in order to minimize cycle time, maintain constant grinding temperatures, minimize wheel wear, or even for a design of multi-grit wheel with improved performance (e.g. minimum variation of the maximum undeformed chip-thickness for the given line-aggressiveness along the wheel profile).

In order to validate the application of the theory of aggressiveness, the grinding specific-energy was determined from crankpin-grinding experiments [24]. Here, the grinding power was measured for various infeeds and the specific energy was calculated using the material-removal rate (Table 1). The experiments were conducted in two independent steps: 1) grinding of cylindrical bearing surface where only radial infeed was varied ($a_x = 0.01 - 0.15$ mm); and 2) grinding of sidewall via variation of the axial feed ($a_z = 0.005 - 0.05$ mm). A vitrified-bond B151-grit-size CBN wheel was used on a heavy-duty CNC crankshafts grinder (Fig. 7a). Workpiece material was 38MnSiVS5 micro-alloyed carbon steel, induction hardened to 53–59 HRC. Coolant used was emulsion at 6% concentration delivered at approximately 1.5 MPa pressure and 350 l/min flow rate. Dressing was performed using a diamond roll with the following parameters: dressing depth of 5 µm, dressing overlap ratio in the range of 3–4, and dressing velocity ratio of +0.8. These parameters give a dressing aggressiveness-number of $Aggr_D = 0.007$.

The obtained grinding specific-energy is presented in two ways: 1) plotted vs. an established grinding parameter – the equivalent chip-thickness, $h_{eq,G}$ (Fig. 9a); and 2) plotted vs. the grinding aggressiveness-number, $Aggr_G$(Fig. 9b). In grinding the bearing surface, the grinding aggressiveness number is determined as $Aggr_G = Aggr'_w(s = 0)$, whereas in grinding the sidewall surface it is $Aggr_G = Aggr'_w(s = s_{\max})$. The equivalent chip-thickness is calculated from the equation given in Table 1. Based on Fig. 9b, it is evident that the aggressiveness number fully captures the geometry and kinematics of the process, reflected by near 1 coefficient of determination. In contrast, plotting the specific energy vs. commonly used process parameters that

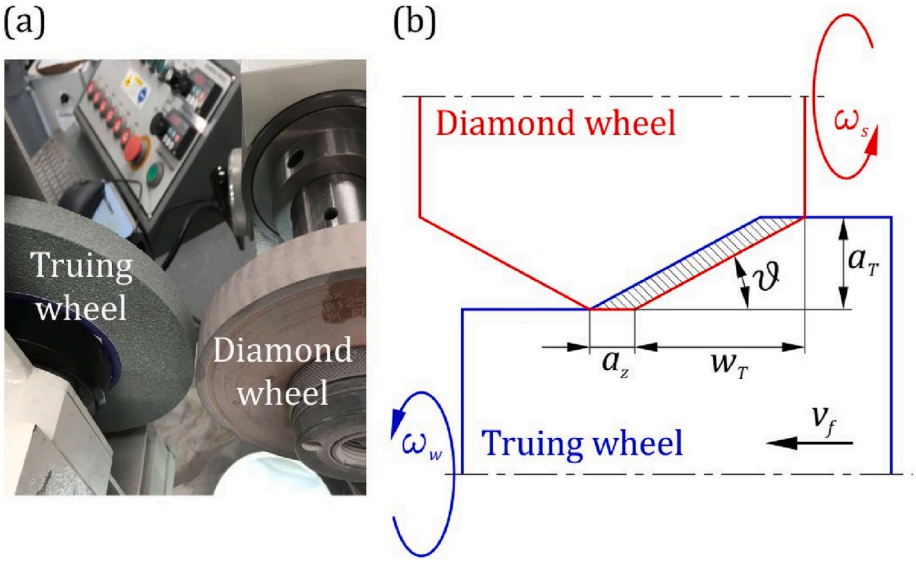

Fig. 10. (a) Diamond-wheel truing with (b) illustration and parameters.

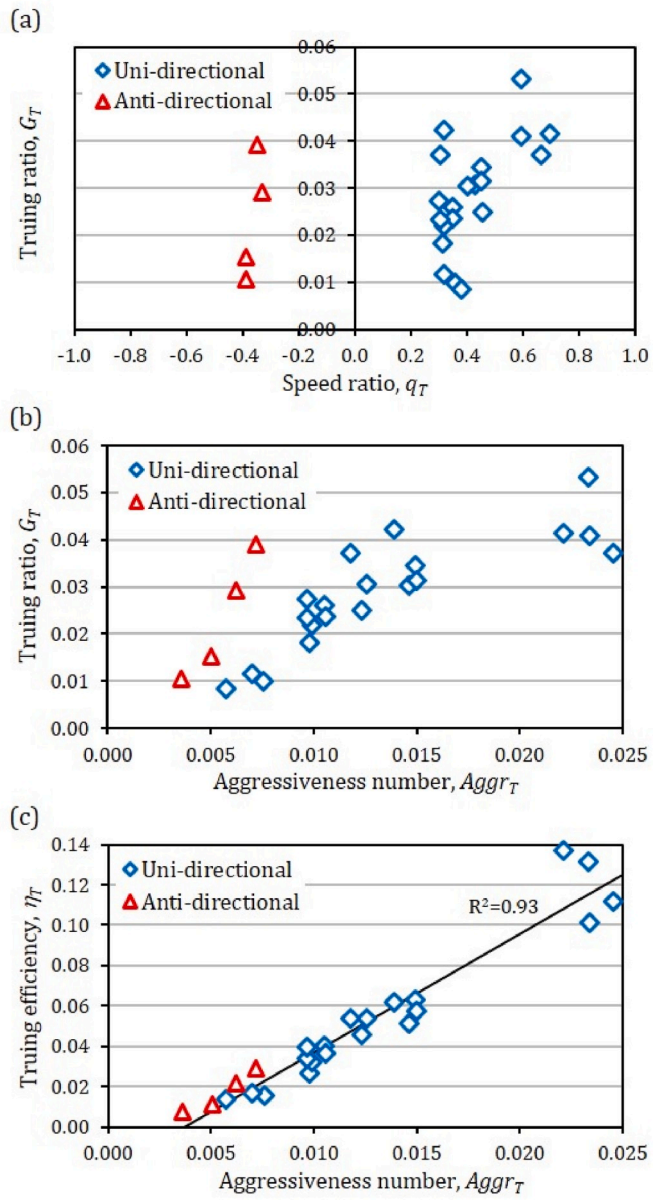

Fig. 11. Truing ratio vs. (a) speed-ratio and (b) aggressiveness number, and (c) truing efficiency vs. aggressiveness number.

do not fully incorporate geometry and kinematics, such as $h_{eq,G}$ (Fig. 9a), may lead to false interpretation of observed deviations in measured outputs.

3.2. Truing of diamond wheels

Truing is a pre-grinding conditioning (shaping) of a grinding wheel that encompasses removing a portion of the diamond grinding wheel using a truing wheel (Fig. 10a). Because of diamond's extreme hardness, the wear of the truing wheel is much larger than the consumption of the diamond wheel. For this reason, the roles in modelling the truing process are reversed (Table 4), meaning the diamond wheel is considered as an abrasive tool and the truing wheel as a workpiece [25]. An efficiency of the truing process depends on removal/wear mechanism, which is the subject of observation in this case-study.

In truing, a truing wheel is traversed over a diamond wheel at a set truing depth, a_T, and traverse velocity, v_f, with infeed before both the forward and the reverse stroke. The traverse operation is adapted to the context of the theory of aggressiveness by assuming a uniform wear of the diamond wheel within the truing width, w_T, resulting in a taper at both sides of the diamond wheel (Fig. 10b), which is seen in practice. In this way, the axial infeed is determined as a truing lead: $a_z = 2\pi v_f/\omega_w$. The other geometrical variables required by the theory of aggressiveness are: $\alpha = 0,\ \vartheta = a_T/w_T \Rightarrow C_{\sin} = a_T/w_T,\ C_{\cos} = 1$ and $\rho \to \infty$. Note that the conditions within the abrasive contact do not change along the wheel profile. Therefore, in this case the definition of the profile position, s, is not necessary.

Using the equations given in the theoretical section, the depth of cut from both perspectives at truing is obtained as:

$$a_s = a_w = a_n = a_z \frac{a_T}{w_T}, \tag{35}$$

and the aggressiveness number at truing, together with the line-aggressiveness from both perspectives, is:

$$Aggr_T = Aggr_s^{'} = Aggr_w^{'} = \frac{1}{|1-q_T|}\sqrt{\frac{a_z}{2r_{eq}}\frac{a_T}{w_T}}. \tag{36}$$

Small values of the speed ratio, q_T, characteristic for truing mean that the diamond-wheel speed is close to the truing-wheel speed. This results in aggressiveness numbers that are typically two orders of magnitude greater (100x) than those in typical grinding processes.

The objective of truing is to remove diamond grits using the truing wheel, which is a challenging task considering the extreme hardness of diamond. The main output of the truing process is the truing ratio, G_T, defined as the quotient between the volume of diamond wheel removed (diamond and bond and porosity) to the volume of truing wheel consumed (grit and bond and porosity). Unfortunately, as shown in Ref. [25], the truing ratio does not accurately quantify the removal efficiency of the truing interaction. Assuming two different relative speeds and the same removal efficiency, a larger amount of diamond grits per consumed volume of the truing wheel would be removed at larger relative speed because a larger number of grits is active within the abrasive contact. Therefore, in order to exclude the effect of relative speed, the truing efficiency [25] is defined as:

$$\eta_T = G_T / |1-q_T| \tag{37}$$

To validate the applicability of the theory of aggressiveness, the truing ratio was measured for various combinations of truing inputs. Experimental work included truing a 180-mesh, resin-bonded, 125-concentration, R-grade diamond wheel (diameter 150 mm, width 17.8 mm, speed range 2.3–10.9 m/s) with a 120-mesh, J-grade Al_2O_3 truing wheel (diameter range 145–201 mm, width 13.2 mm, speed range 7.7–15.7 m/s), rotating in the same (uni-directional) or the opposite direction (anti-directional), at different truing depths (0.013–0.051 mm) and traverse velocities (8.3–33.3 mm/s). To quantify the volumetric changes with respect to diamond and truing wheels, an optical system and special micrometer were used, respectively.

First, the measured truing ratio shown in Fig. 11a is plotted vs. the speed ratio. This correlation reveals no insight into the truing process. Next, the truing ratio is plotted vs. the aggressiveness number (Fig. 11b). Although some trend that larger aggressiveness numbers give larger truing ratios can be observed, the truing ratio does not capture the effect of different speed ratios in the truing interface. However, plotting the truing efficiency vs. the aggressiveness number (Fig. 11c) results in a distinct linear relationship. Hence, for a given wheel-workpiece, a novel fundamental characteristic is obtained which correlates the geometrical and kinematical inputs via the aggressiveness number with the truing efficiency.

3.3. Dressing of CBN wheels

Diamond dressing is an abrasive process for conditioning the topography (sharpness) of a grinding wheel. In this case-study, a

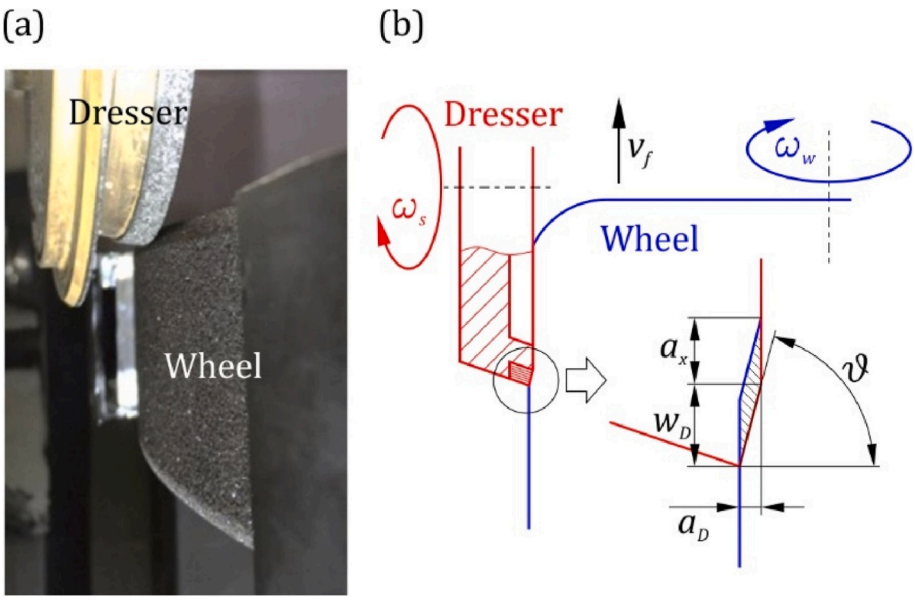

Fig. 12. (a) CBN grinding-wheel dressing with (b) illustration and parameters.

diamond cup-wheel dresser is used for traverse dressing the outer diameter of a CBN grinding wheel (Fig. 12a), which is then used to grind crankshafts. For the modelling purpose, the diamond dresser represents the abrasive tool and the grinding wheel represents the workpiece. Here the theory of aggressiveness is applied to: 1) the dressing specific-energy, determined as a ratio of dressing power and material removal rate, $e_D = P_D/Q_D$; and 2) the grinding wheel topography, evaluated by 2.1) the workpiece surface roughness after grinding, and 2.2) the grinding specific energy when grinding with differently dressed CBN grinding wheels.

Similar to truing – but with vastly different outcomes – dressing is performed by traversing a grinding wheel over a diamond dresser at a specified dressing depth, a_D, and traverse velocity, v_f, typically with infeed before both the forward and the reverse stroke. Again, a uniform wear of the dresser within the dressing width, w_D, is assumed, resulting in a taper at the edge of the diamond cup-wheel dresser (Fig. 12b). The radial infeed is then determined as a dressing lead: $a_x = 2\pi v_f/\omega_w$. The other geometrical variables required by the theory of aggressiveness are: $\alpha = \pi/2,\ \vartheta = \pi/2 - a_D/w_D \Rightarrow C_{\sin} = r_{eq}/r_s, C_{\cos} = r_{eq}/r_w$ and $\rho \rightarrow \infty$. Again, the conditions within the abrasive contact do not change along the tool profile, and the definition of the profile position, s, is not necessary.

The depth of cut from both perspectives is given based on the equations in the theoretical section as:

$$a_s = a_w = a_n \frac{r_w}{r_{eq}} = a_x \frac{a_D}{w_D} \frac{r_w}{r_{eq}}. \tag{38}$$

Moreover, the aggressiveness number at dressing, together with the line-aggressiveness from both perspectives, is:

$$Aggr_D = Aggr_s^{'} = Aggr_w^{'} = \frac{1}{|1 - q_D|} \sqrt{\frac{a_x}{2r_w} \frac{a_D}{w_D}}. \tag{39}$$

Just like truing, the dresser speed is typically close to a grinding wheel speed, resulting in aggressiveness numbers that are around 100-times larger than those in grinding.

Dressing experiments were performed on the same CNC machine used in the crankshaft-grinding case study, with the same CBN wheel and speed ($r_w = 350$ mm, $v_w = 70$ m/s) and diamond cup-wheel dresser ($r_s = 79$ mm, $w_D = 0.85$ mm). Different dressing conditions were achieved by combining the following values of dressing parameters: 1) two values of the speed ratio (0.43 and 0.86), achieved by changing the dresser speed; 2) two values of dressing depth (0.002 mm and 0.006 mm); and 3) three values of the traverse velocity (2 mm/s, 5 mm/s and 12 mm/s).

The dressing specific-energy, obtained from the measured dressing power and calculated dressing material-removal rate (Table 1), is plotted vs. three geometrical-kinematical parameters: the specific material-removal rate (Fig. 13a), the equivalent chip-thickness (Fig. 13b) and the aggressiveness number (Fig. 13c). Again, it is evident that specific energy correlates with the aggressiveness number as a single-valued function.

The next application of theory of aggressiveness is unique: applying the aggressiveness number in dressing to results measured in grinding – after dressing with different parameters. Here the bearing surface of a crankpin was plunge-ground after dressing the wheel. Grinding tests were performed at the same grinding conditions ($a_x = 0.02$ mm, $v_s = 70$ m/s, $v_w = 223$ mm/s), which give a grinding aggressiveness number of 4.7E-5. As already mentioned, the objective of the grinding tests is to indirectly correlate the dressing aggressiveness number with the wheel sharpness.

First, the measured surface roughness after grinding, Ra_G, is plotted vs. the dressing aggressiveness-number (Fig. 14a). Here, only a general trend of larger aggressiveness number giving a rougher surface can be observed. However, if the findings from the truing efficiency definition (Eq. (37)) are used, it could be assumed that larger dressing relative speeds at the same dressing aggressiveness number would give a smoother grinding wheel due to a larger number of abrasive interactions. In this way, the equivalent grinding roughness, which would exclude the effect of the dressing relative-speed, is defined as:

$$Ra_{eq,G} = Ra_G/|1 - q_D|. \tag{40}$$

The given assumption is confirmed by Fig. 14b, where a linear

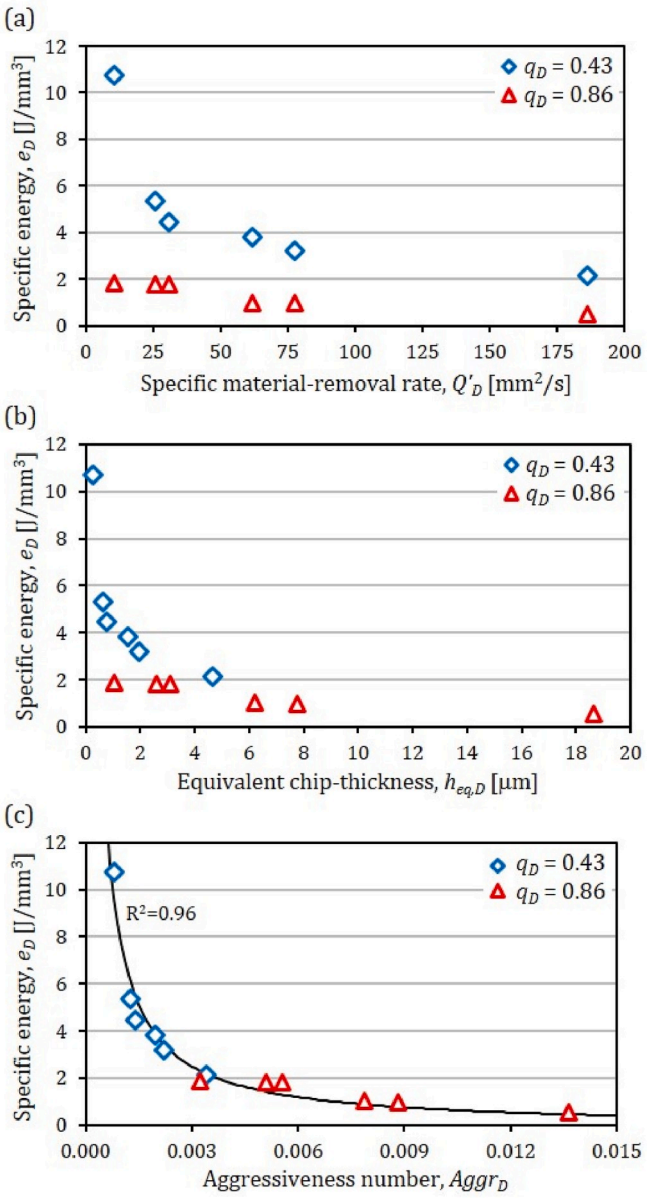

Fig. 13. Dressing specific-energy vs. (a) specific material-removal rate, (b) equivalent chip-thickness and (c) aggressiveness number.

relation between the dressing aggressiveness number and the equivalent grinding roughness is obvious.

Similar conclusions could be drawn by observing the grinding specific-energy vs. the dressing aggressiveness-number. Following the same argumentation, a smoother grinding wheel, which corresponds to larger dressing relative-speed, would give larger grinding specific-energy. In this case, the equivalent grinding specific-energy is defined as:

$$e_{eq,G} = e_G|1 - q_D|. \tag{41}$$

The grinding specific-energy (Fig. 15a) and the equivalent grinding specific-energy (Fig. 15b) are plotted vs. the dressing aggressiveness-number. Here, the equivalent grinding specific-energy also correlates with the dressing aggressiveness-number as a single-valued function. By this, a fundamental nature of the theory of aggressiveness in terms of process geometry and kinematics is confirmed once more.

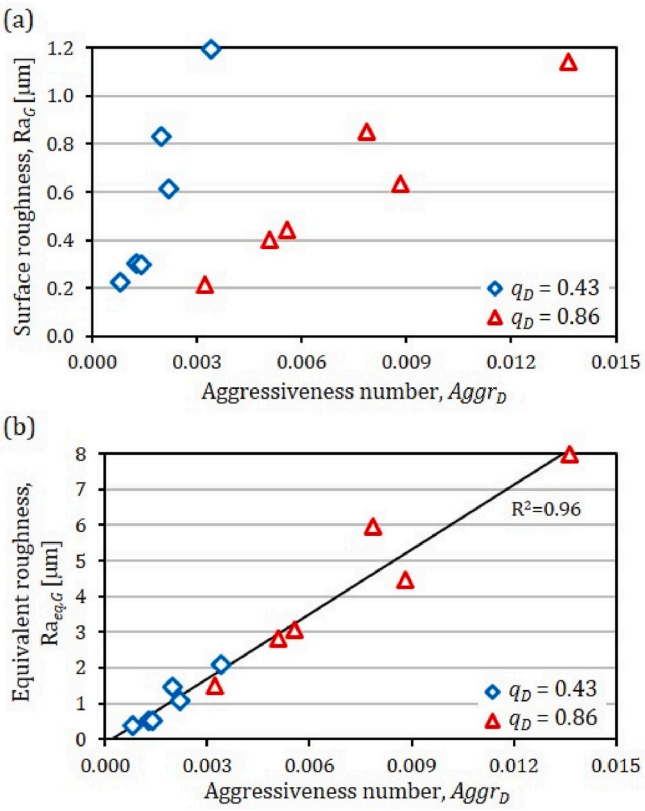

Fig. 14. (a) Surface roughness and (b) equivalent roughness after grinding vs. aggressiveness number of dressing.

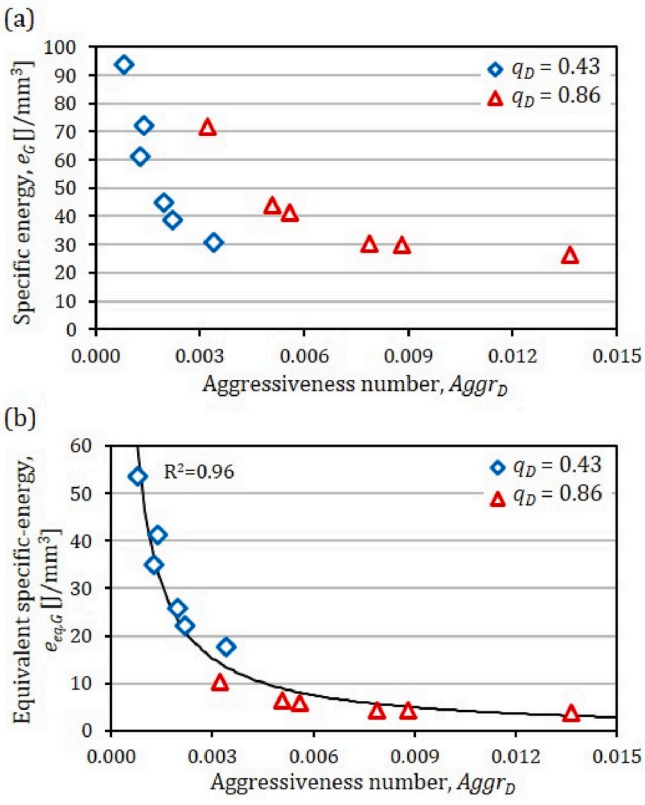

Fig. 15. (a) Specific energy and (b) equivalent specific-energy of grinding vs. aggressiveness number of dressing.

4. Conclusions

The objective of this work has been to develop and promote a novel theory for analytical modelling of abrasive processes. This unifying concept, termed the theory of aggressiveness, quantifies the fundamental mechanics of any abrasive interaction for any arbitrary process geometry and kinematics. The theory of aggressiveness comprises several dimensionless parameters with the following unique features:

- The point-aggressiveness, $Aggr^*$, quantifies an interaction between the abrasive tool and the workpiece in terms of geometry and kinematics at any given point on the abrasive-tool surface.
- The line-aggressiveness, $Aggr^{'}$, brings the point-aggressiveness to the abrasive contact as a function of the abrasive-tool profile position. The line-aggressiveness distribution can be considered fundamental to the study of various physical aspects of an abrasive process.
- The aggressiveness number, $Aggr$, gives the overall geometrical-kinematical characteristic of the abrasive contact quantifying the abrasive interaction.

The application of the theory of aggressiveness demonstrates its unifying nature by the following experimentally obtained findings:

- The theory of aggressiveness is applied to various abrasive processes, from high speed-ratio processes (grinding) to low speed-ratio processes (truing, dressing).
- The main advantage of the dimensionless approach is that the value of the aggressiveness parameter itself brings information about the abrasive process: the aggressiveness number in grinding is typically on the order of 10^{-5} to 10^{-4}, whereas the aggressiveness number in truing or dressing is on the order of 10^{-3} to 10^{-2}.
- The characteristic outputs of an abrasive process (i.e. specific energy, abrasive-tool wear and surface roughness) are correlated with the aggressiveness number as fitted single-valued functions, with values of the coefficient of determination, R^2, near 1 for all the cases demonstrated: 0.999 for grinding, 0.93 for truing and 0.96 for dressing.

The results of this work will (hopefully) revitalize the modelling subject area and provide the theoretical foundation for future analyses and optimization of abrasive processes.

Declaration of competing interest

The authors declare that they have no known competing financial interests or personal relationships that could have appeared to influence the work reported in this paper.

CRediT authorship contribution statement

Radovan Dražumerič: Conceptualization, Methodology, Formal analysis, Visualization, Writing - original draft. **Jeffrey Badger:** Conceptualization, Investigation, Validation, Writing - review & editing. **Roope Roininen:** Investigation, Resources. **Peter Krajnik:** Conceptualization, Writing - review & editing, Supervision, Project administration, Funding acquisition.

Acknowledgements

This work was funded by the International Grinding Institute (IGI), Scania CV AB and Chalmers University of Technology.

References

[1] M.E. Merchant, Mechanics of the metal cutting process. I. Orthogonal cutting and a type 2 chip, J. Appl. Phys. 16 (1945) 267–275, https://doi.org/10.1063/1.1707586.
[2] M.C. Shaw, Plastic flow in the cutting and grinding of materials, Proc. Natl. Acad. Sci. U.S.A. 40 (1954) 394–401, https://doi.org/10.1073/pnas.40.6.394.
[3] P.L.B. Oxley, Mechanics of metal cutting, Int. J. Mach. Tool Des. Res. 1 (1961) 89–97, https://doi.org/10.1016/0020-7357(61)90046-4.
[4] B. Linke, F. Klocke, Temperatures and wear mechanisms in dressing of vitrified bonded grinding wheels, Int. J. Mach. Tool Manufact. 50 (2010) 552–558, https://doi.org/10.1016/j.ijmachtools.2010.03.002.
[5] T. Tawakoli, B. Azarhoushang, Intermittent grinding of ceramic matrix composites (CMCs) utilizing a developed segmented wheel, Int. J. Mach. Tool Manufact. 51 (2011) 112–119, https://doi.org/10.1016/j.ijmachtools.2010.11.002.
[6] S. Agarwal, P.V. Rao, Predictive modeling of force and power based on a new analytical undeformed chip thickness model in ceramic grinding, Int. J. Mach. Tool Manufact. 65 (2013) 68–78, https://doi.org/10.1016/j.ijmachtools.2012.10.006.
[7] T.T. Öpöz, X. Chen, Experimental investigation of material removal mechanism in single grit grinding, Int. J. Mach. Tool Manufact. 63 (2012) 32–40, https://doi.org/10.1016/j.ijmachtools.2012.07.010.
[8] C. Dai, W. Ding, J. Xu, Y. Fu, T. Yu, Influence of grain wear on material removal behavior during grinding nickel-based superalloy with a single diamond grain, Int. J. Mach. Tool Manufact. 113 (2017) 49–58, https://doi.org/10.1016/j.ijmachtools.2016.12.001.
[9] U. Karagüzel, E. Uysal, E. Budak, M. Bakkal, Analytical modeling of turn-milling process geometry, kinematics and mechanics, Int. J. Mach. Tool Manufact. 91 (2015) 24–33, https://doi.org/10.1016/j.ijmachtools.2014.11.014.
[10] G.I. Alden, Operation of grinding wheels in machine grinding, Trans. ASME 36 (1914) 451–460.
[11] J.J. Guest, Grinding Machinery, Edward Arnold, London, 1915.
[12] J.A. Badger, A.A. Torrance, A comparison of two models to predict the grinding force from wheel surface topography, Int. J. Mach. Tool Manufact. 40 (2000) 1099–1120, https://doi.org/10.1016/S0890-6955(99)00116-9.
[13] S. Malkin, C. Guo, Grinding Technology, Theory and Applications of Machining with Abrasives, Industrial Press Inc., New York, 2008.
[14] H.K. Tönshoff, J. Peters, I. Inasaki, T. Paul, Modelling and simulation of grinding processes, CIRP Ann. - Manuf. Technol. 41 (1992) 677–688, https://doi.org/10.1016/S0007-8506(07)63254-5.
[15] R. Snoeys, J. Peters, The significance of chip thickness in grinding, CIRP Ann. - Manuf. Technol. 23 (1974) 227–237.
[16] G.S. Reichenbach, J.E. Mayer, S. Kalpakcioglu, M.C. Shaw, The role of chip thickness in grinding, Trans. ASME 78 (1956) 847–860.
[17] Y. Zhang, C. Fang, G. Huang, X. Xu, Modeling and simulation of the distribution of undeformed chip thicknesses in surface grinding, Int. J. Mach. Tool Manufact. 127 (2018) 14–27, https://doi.org/10.1016/j.ijmachtools.2018.01.002.
[18] J.N. Brecker, M.C. Shaw, Measurement of the effective number of cutting points in the surface of a grinding wheel, in: Proceeding of the International Conference on Production Engineering, Japan Society of Precision Engineers, Tokyo, 1974, pp. 740–745.
[19] S. Malkin, T. Murray, Mechanics of rotary dressing of grinding wheels, J. Eng. Ind. Trans. ASME 100 (1978) 95–102, https://doi.org/10.1115/1.3439353.
[20] A. Spampinato, D.A. Axinte, On modelling the interaction between two rotating bodies with statistically distributed features: an application to dressing of grinding wheels, Proc. R. Soc. A 473 (2017) 20170466, https://doi.org/10.1098/rspa.2017.0466.
[21] R. Holtermann, A. Menzel, S. Schumann, D. Biermann, T. Siebrecht, P. Kersting, Modelling and simulation of Internal Traverse Grinding: bridging meso- and macro-scale simulations, Prod. Eng. Res. Dev. 9 (2015) 451–463, https://doi.org/10.1007/s11740-015-0613-z.
[22] G.J. Pietsch, M. Kerstan, Understanding simultaneous double-disk grinding: operation principle and material removal kinematics in silicon wafer planarization, Precis. Eng. 29 (2005) 189–196, https://doi.org/10.1016/j.precisioneng.2004.07.001.
[23] P. Krajnik, R. Dražumerič, J. Badger, F. Hashimoto, Cycle optimization in cam-lobe grinding for high productivity, CIRP Ann. - Manuf. Technol. 63 (2014) 333–336, https://doi.org/10.1016/j.cirp.2014.03.036.
[24] R. Dražumerič, R. Roininen, J. Badger, P. Krajnik, Temperature-based method for determination of feed increments in crankshaft grinding, J. Mater. Process. Technol. 259 (2018) 228–234, https://doi.org/10.1016/j.jmatprotec.2018.04.032.
[25] R. Dražumerič, J. Badger, U. Klement, P. Krajnik, Truing of diamond wheels – geometry, kinematics and removal mechanisms, CIRP Ann. - Manuf. Technol. 67 (2018) 345–348, https://doi.org/10.1016/j.cirp.2018.04.091.
[26] D. Barrenetxea, J. Alvarez, J.I. Marquinez, J.A. Sanchez, Grinding with controlled kinematics and chip removal, CIRP Ann. - Manuf. Technol. 65 (2016) 341–344, https://doi.org/10.1016/j.cirp.2016.04.097.
[27] C. Guo, Y. Chen, Thermal modeling and optimization of interrupted grinding, CIRP Ann. - Manuf. Technol. 67 (2018) 321–324, https://doi.org/10.1016/j.cirp.2018.04.083.
[28] Y. Wang, Y. Liu, X. Chu, Y. He, W. Zhang, Calculation model for surface roughness of face gears by disc wheel grinding, Int. J. Mach. Tool Manufact. 123 (2017) 76–88, https://doi.org/10.1016/j.ijmachtools.2017.08.002.